Geoffrey Z. Iwata, Yinan Hu*, Arne Wickenbrock, Tilmann Sander, Muthuraman Muthuraman*, Venkata Chaitanya Chirumamilla, Sergiu Groppa, Qishan Liu and Dmitry Budker

Biomagnetic signals recorded during transcranial magnetic stimulation (TMS)-evoked peripheral muscular activity

https://doi.org/10.1515/bmt-2021-0019
Received January 23, 2021; accepted July 11, 2022;
published online August 15, 2022

Abstract: Transcranial magnetic stimulation (TMS) has widespread clinical applications from diagnosis to treatment. We combined TMS with non-contact magnetic detection of TMS-evoked muscle activity in peripheral limbs to explore a new diagnostic modality that enhances the utility of TMS as a clinical tool by leveraging technological advances in magnetometry. We recorded measurements in a regular hospital room using an array of optically pumped magnetometers (OPMs) inside a portable shield that encloses only the forearm and hand of the subject. We present magnetomyograms (MMG)s of TMS-evoked movement in a human hand, together with a simultaneous surface electromyograph (EMG) data. The biomagnetic signals recorded in the MMG provides detailed spatial and temporal information that is complementary to that of the electric signal channels. Moreover, we identify features in the magnetic recording beyond that of the EMG. This system demonstrates the value of biomagnetic signals in TMS-based clinical approaches and widens its availability and practical potential.

Keywords: biomagnetic signals; magnetomyograms; optically pumped magnetometers; transcranial magnetic stimulation.

Introduction

The central nervous system of the human body forms a critical signaling network that controls over 200 muscles [1]. Developing new technologies that aid in understanding and measuring the nerve-innervation patterns and muscle activity controlled by this network is crucial for the advancement of research, diagnosis and treatment of motor-system diseases like Parkinson's disease and amyotrophic lateral sclerosis (ALS) [2, 3]. Recently, transcranial magnetic stimulation has gained widespread use for the research and diagnosis of various neuropsychiatric disorders [4–8]. In TMS, a strong pulse of magnetic field can be applied to different cortical areas. When applied to the motor cortex, TMS results in an evoked muscle response in the form of a 'twitch' [9–11]. TMS offers a safe, controlled, and non-invasive method to investigate the motor pathways, making it an ideal platform for studying central motor conduction activity [12–14]. Electrophysiological measurement techniques such as electromyography [15] are used as a gold-standard tool to study neural and muscle activity in descending motor waves evoked by TMS. During an electromyogram, surface or needle electrodes record differences in electric potential in periphery limbs, but the magnetic signals that accompany electrophysiological signals can provide additional crucial clinical information about innervation and muscle activity that is spatially and temporally well resolved [16, 17].

Biomagnetic measurements can offer complementary data in TMS-EMG experiments aiming to measure motor evoked potentials. Surface electrical potential measurements

Yinan Hu: co-first author.

Geoffrey Z. Iwata and Yinan Hu contributed equally to this work.

***Corresponding authors: Yinan Hu,** Johannes Gutenberg-Universität Mainz, 55128 Mainz, Germany; and Helmholtz-Institut Mainz, GSI Helmholtzzentrum für Schwerionenforschung, 55128 Mainz, Germany, E-mail: yinanhu1@uni-mainz.de; and **Muthuraman Muthuraman,** Department of Neurology, Biomedical Statistics and Multimodal Signal Processing Unit, University Medical Center of the Johannes Gutenberg-University Mainz, Mainz 55131, Germany, E-mail: mmuthura@uni-mainz.de. https://orcid.org/0000-0001-6158-2663
Geoffrey Z. Iwata and Arne Wickenbrock, Johannes Gutenberg-Universität Mainz, Mainz, Germany; and Helmholtz-Institut Mainz, GSI Helmholtzzentrum für Schwerionenforschung Mainz, Germany
Tilmann Sander, Physikalisch-Technische Bundesanstalt, Berlin, Germany
Venkata Chaitanya Chirumamilla and Sergiu Groppa, Department of Neurology, Biomedical Statistics and Multimodal Signal Processing Unit, University Medical Center of the Johannes Gutenberg-University Mainz, Mainz, Germany
Qishan Liu, Johannes Gutenberg-Universität Mainz, Mainz, Germany
Dmitry Budker, Johannes Gutenberg-Universität Mainz, Mainz, Germany; Helmholtz-Institut Mainz, GSI Helmholtzzentrum für Schwerionenforschung Mainz, Germany; and Department of Physics, University of California, Berkeley, CA, USA

from EMG provide rich data conveying information muscle activity in the vicinity of the electrode with excellent temporal resolution. These potential differences arise due to cell depolarization activity associated with so called, motor unit action potentials (MUAPs), which in turn are a summation of individual muscle action potentials propagating along a single contracted muscle fiber [15]. The surface EMG then, measures not the direct action potential in the muscle, but rather the associated ensemble electric field that reaches the skin at a specific moment in time. Since the electric fields in the body are affected by the conductivity of different tissues and specific skin conditions, it can be challenging to recover the exact origin of the EMG signal without complex and careful electrode placing and analysis of the specific conditions of physiology [18]. Magnetic fields arise from the constellation of electrical activity within the body and thus also require detailed analysis to recover source information. These fields convey information from both the primary MUAPs, as well as the secondary propagation of electrical activity through the surrounding biomass. Nevertheless, detailed array measurements of the field can also be used to locate these primary sources [19]. Importantly, since the relative magnetic permeability of human tissue is close to unity, the magnetic fields from MUAPs are directly related to the electro-chemical activity within muscles, unaffected by specific conditions of the surrounding tissue [20], and crucially, do not rely on a sensor-skin connection. Therefore, in combination with TMS, these magnetic signals can be powerful tools in studying the proper functioning and response of the muscular and central nervous systems [21], forming a crucial complement to both needle and surface electrode measurements, which measure relative electrical potential differences.

Additionally, since the detection of magnetic fields does not require physical contact, magnetic measurements of muscle activity, or, magnetomyography (MMG) is a correspondingly non-contact technique. These aspects make MMG an attractive tool for complementing EMG, since magnetic signals can cross-validate electrophysiological measurements by decoupling signal strength from changes in systematic experimental conditions, such as electrode-skin contact for electrodes. TMS provides ideal conditions for operating these different sensing modalities, because TMS is a repeatable and controlled stimulation, measurements can be triggered and averaged with high accuracy in timing, improving the signal-to-noise ratio and repeatability of biomagnetic signals.

Despite the apparent motivations for magneto-physiological measurements, the very small signal size (<10 pT) has limited widespread adoption of biomagnetic measurements as a routine clinical measurement, since this regime of sensitivity has been limited to SQUIDs [22] (superconducting quantum interference devices), which require liquid helium cooling. As a result, while SQUIDs have been for decades used for detection of biomagnetic signals [16, 23–25], the associated measurement systems are bulky, expensive, and ill-suited to the different geometries of various body parts, limiting these systems' practical utility. Recent developments in atomic magnetometry have led to new, high-sensitivity devices known as optically pumped magnetometers (OPMs) [26–28] that are cryogen-free, centimeter-scale, and relatively low cost – characteristics necessary to make magneto-physiological measurements an accessible diagnostic tool. Current OPM technology mandates heating the sensor, resulting in surface temperatures of around 40 °C. Additionally, OPMs have opportunities and applications in wearable [29], compact devices with wide application outside of clinical use. For these reasons, OPMs have recently generated broad research interest as a viable alternative to SQUIDs in measuring weak biomagnetic signals.

In this work, we leverage the advances in OPM technology to enhance the diagnostic utility of TMS. We combine an extended array of OPMs around the hand of a human subject with a surface electromyograph to provide a comparison of techniques. Recent work has shown that OPMs can detect electrically stimulated muscle activity in the hand and foot while in a shielded room environment [30–32]. In contrast, our TMS-evoked activity arises from signals that are evoked at the motor cortex and we compare MMG and EMG. Thus, we extend magnetic measurements to regularly performed clinical routines that study TMS-evoked activity and we achieve that in a regular hospital examination room, using a portable magnetic shield that only encompasses the arm of the subject. This circumvents the need for a large and expensive magnetically shielded room. We show biomagnetic signals with features that are not present in EMG measurements. These results show an investigation of OPM-recorded evoked muscle activity from repetitive TMS, with the realization of local magnetic shielding for human biomagnetic measurements in a clinical setting. This OPM-TMS platform also opens new possibilities for identifying nerve transmission pathways and external detection of voluntary motor responsesusing a similar simple setting.

Methods

Subjects

All measurements were repeated for four healthy subjects in total, between ages 26 and 40, who volunteered for the study and signed

informed consent. All subjects are right-handed and have no severe somatic diseases or any mental or neurological diseases with confirmed diagnosis. Written informed consent in accordance with the Declaration of Helsinki was obtained from all subjects before participation in this study, which was approved by the Ethics Committee of the State Medical Association of Rhineland-Palatine. Written informed consent was also obtained from all subjects to publish data/images relating to the experiment in an online open-access publication.

Experimental procedure

The OPM and EMG electrode configurations within the shield are shown in Figure 1A, B. The measurement preparation time, including control measurements, takes less than 30 min. The biomagnetic signal is recorded with an array of four OPMs below the hand and an additional four above the hand, while the EMG is simultaneously recorded to correlate and provide reference for the signals. We used disposable surface adhesive EMG electrodes from Neurotab (Spes Medica) to avoid any artifact on the magnetic recordings. The EMG electrodes used were in 250 cm in length so the connection to the EMG amplifier was far away from the magnetic recordings there was no noise due to the electrode cables as the hand was also fixed on the chamber.

For each participant, the magnetomyography magnetometers and the EMG surface electrodes were prepared and tested individually with the data acquisition system. Additionally EEG was recorded, and the results are shown below. The EMG was recorded using one channel of a 256-channel EGI system (Electrical Geodesics, Inc.) and synchronized with OPM's using a trigger signal from the TMS pulse. The subject's hand was positioned in the shield, and the TMS coil was positioned over the subject's left M1 region (Figure 1C). The stimulation was applied at different frequencies 0.5, 3, and 9 Hz for a maximum of up to 3 min depending on the comfort of the subject.

The TMS pulse results in a strong magnetic field (≈1.4 T) on the motor cortex of the participant, which is less than a meter away from the EMG and MMG sensor positions. The sensors record a magnetic artifact arising from the TMS pulse, which consists of a bi-phasic pulse lasting approximately 300 μs. To identify and isolate this artifact, a control measurement was performed in which each participant moved their head down (Figure 1D) and data was taken for same stimulation described above. Since the high-intensity and rapidly changing region of the magnetic field from the TMS is highly localized, the induced electrical field and resulting brain activity is also limited to a small volume. Therefore, the participants' change in head position results in there being no discernible evoked effect. No motor evoked potential is observed on the EMG, and a lack of a 'twitch' in the hand was confirmed using a

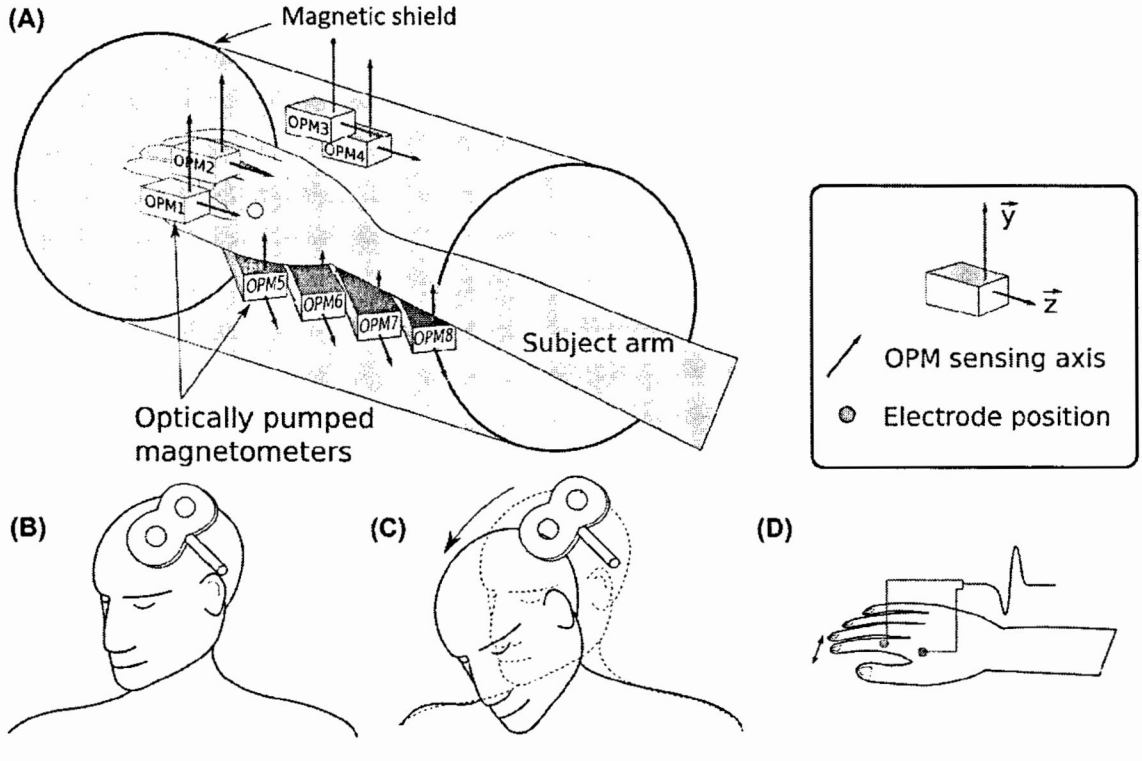

Figure 1: Experimental setup.
(A) Schematic of a subject's hand within the innermost magnetic shield layer. Sensor positions of the magnetometers and electrodes are indicated. Not indicated are mounting/supporting elements or wires. (B) Schematic of a participant's head with a TMS coil positioned over the motor cortex. (C) Control measurement to identify magnetic artifacts in sensor output arising from the TMS pulse. When the participants moves the head down, the TMS coil is unable to stimulate the motor cortex. (D) Muscle evoked potentials (MEP) were recorded from right first dorsal interosseus (FDI) muscle during TMS. The stimulus results in a lateral 'twitch' of the right index finger.

camera aimed through an access port on the shield. These measurements showed that this artifact lasts up to 15 ms on the averaged OPM signal – distorted 50 times longer than the true pulse due to a combination of low pass filtering in the sensor hardware and the low sampling rate.

Transcranial magnetic stimulation (TMS)

To administer TMS, a stimulation coil is placed over of the target area of a participant's scalp, to determine the TMS coil position and orientation is important, we move the TMS coil until the EMG's response is shown clearly, then we position the TMS coil with mechanical arm, the subjects need to stand still during whole period. The coil orientation was fixed to 30° based on previous literature to elucidate optimal MEP responses [33]. A strong electrical current running through the coil results in a region of rapidly changing, intense magnetic field within the participant's brain. This pulsed magnetic field induces a secondary electrical current within the cortical tissue, which, if within the motor cortex, may result in muscular activation [34]. The muscle activity can be detected via electromyography, and the resulting signal is known as a motor evoked potential [35].

The Magstim Super Rapid 2 stimulator (Magstim, UK) with a figure-of-eight coil with internal winding diameter of 70 mm was used. The TMS pulse had a bi-phasic waveform and was applied at the left primary motor cortex M1 with an intensity of 110% of the subjects resting motor threshold (RMT) (Figure 1B). The RMT was determined as the minimum stimulus intensity required to elicit motor evoked potentials of amplitude 50 μV in 5 out of 10 consecutive trials at rest in the contralateral first dorsal interosseous (FDI) muscle (Figure 1D) [13].

Optically pumped magnetometry in a portable shield

Detection of biomagnetic signals requires magnetic sensitivities better than 1 pT/$\sqrt{\text{Hz}}$. The commercially available OPMs (QuSpin) used in this work can achieve a noise floor of 15 fT/$\sqrt{\text{Hz}}$ with a bandwidth between 1 and 100 Hz. These sensors operate by optically probing the zero-field resonance of spin-polarized Rubidium atoms, which is highly sensitive to small magnetic fields [27].

The drawback of this magnetometry approach is a limited dynamic range, requiring a magnetically compensated or shielded background environment in order to reach the sensitivity limits, especially when considering a magnetically hostile hospital setting. Previous human biomagnetic measurements using OPMs were, for the most part, conducted in magnetically shielded rooms (MSRs) which typically have residual fields of <10 nT, magnetic gradients on the order of 1 nT/m [36], and enough space to comfortably accommodate a subject. These characteristics constitute an appropriate working environment for OPMs, allowing low noise measurements and some freedom to move the sensors by 1–2 cm [37]. However, MSRs are expensive and decidedly not portable, which ultimately restricts the OPM technology to the same limitations as SQUID devices. Furthermore, the isolated MSR environment can be unsuitable for subjects to remain inside for long measurement times. Importantly, the large magnetic field generated by TMS could magnetize and negatively affect the shielding.

To circumvent these practical issues associated with MSRs, we instead use a small-sized shield that encompasses only the body part relevant to the measurement. Since we are measuring nerve and muscle activity in the hand, the arm of the subject is placed inside a commercially available four-layer cylindrical shield (Twinleaf MS-2) with one set of end-caps removed. The missing end-cap compromises the DC shielding factor by about a factor of 10 within the sensor region, however, DC magnetic field offsets (<50 nT at sensor positions) arising in the shield can be compensated for with the QuSpin sensor's self-compensation coils. OPMs of the manufacturer used here have internal triple-axis compensation coils, which are energized by the control electronics of each sensor individually. This procedure is started by the user before taking data. These internal coils allow to operate the OPMs even with one end cap removed. Nevertheless, the open shield modification makes the low-field region susceptible to environmental magnetic noise, therefore the ability to average over multiple trials is crucial for retaining a high SNR.

Since magnetic field gradients can be relatively large with an open shield, the sensors must be protected from vibrations or any movement, particularly those that may accompany the invoked muscle activity. Therefore, the subject rests their arm on a custom plastic mold (shown in Figure 2A, B) which is suspended from an aluminum support that extends into the shielded region, but is otherwise disconnected from the shield and sensors. As can be seen in Figure 2. The down OPM array touches the skin, the top OPM array is 9 cm from the center of the subject's arm since the inner diameter of the MS-2 shield is 18 cm. The subject is thus able to make small movements of their hand within the shield without physical disturbance to the sensors and causing false signals. This was verified using control measurements in which the suspended mold and mount were moved at the expected trigger frequency without a subject arm inside. The plastic mold could help to keep the distance between the arm to the sensors are similarly equal to 1.5 cm, for all the sensors at up and down positions.

Environmental magnetic changes in a hospital setting were measured using a fluxgate magnetometer placed outside the shield (Figure 1B), and while large features (>100 nT on fluxgate) were visible on the OPMs, these artifacts were generally sufficiently shielded as to not cause the sensor output to go out of range during the measurement. The effects of these low-frequency transient offsets can be minimized by subtracting sensor signals (software gradiometry) and through averaging.

Eight commercial OPM sensors (QuSpin QZFM – 4× Gen-2, 2× Gen-1.5, 2× Gen-1) are used. Each sensor has two magnetically sensitive axes with separate outputs, resulting in a total of 16 magnetic sensor channels, the only difference for different version of QuSpin magnetometers are their length, besides, they have same performance and sensitivity region. Relevant photographs of the experimental equipment and setup are shown in Figure 2. The OPMs used in this study represent two different versions supplied by the manufacturer. The difference is only housing size and support electronics, the intrinsic properties such as sensitivity, dynamic range, and bandwidth are identical as quoted on the technical information provided by the company. The sensing volume is laterally shifted by 3 mm between the sensor generation. Compared to the cm-range of separation between source and sensors this is negligible. The hand was placed such that FDI is aligned with the positions of OPM1-4. OPMs have an intrinsic low pass 3 dB cut-off point at 150 Hz and an acquisition rate of 1 kHz was chosen synchronous with EEG and EMG. No filter besides the Nyquist filter was applied. Two sensors below (OPM 1 and OPM 4) and two sensors above (OPM 5 and OPM 7) the arm worked consistently for all subjects and were operated in dual-axis mode with sensing axes indicated in Figure 1. In total eight signals are therefore reported for each subject. Sensors closer to the opening of the shield experience

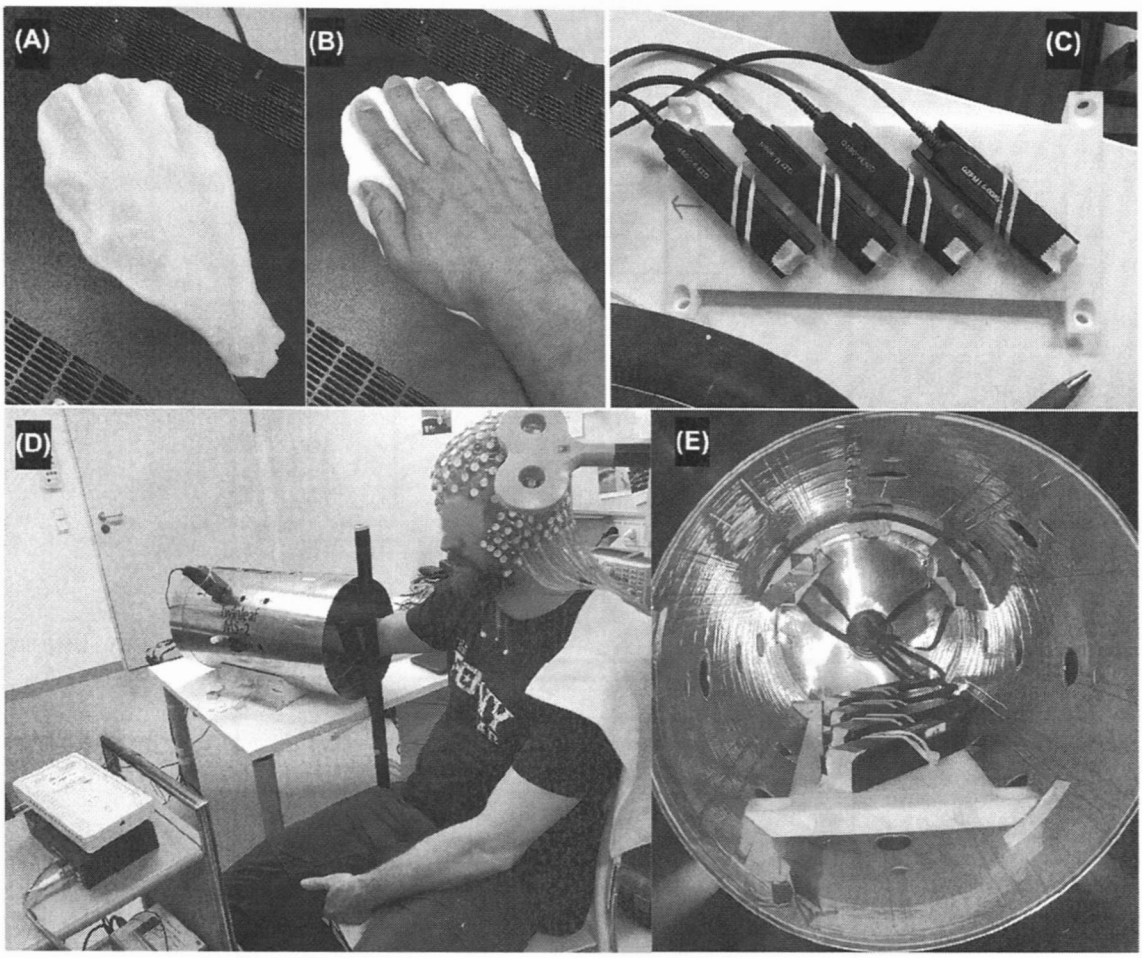

Figure 2: Experiment setup.
(A) Thermo-plastic hand molds made for each subject to rest their forearm and hand on during the measurement. The plastic is molded around an aluminum support for the forearm. The mold section for the index finger is widened to allow for invoked motion due to the TMS. (B) Hand mold with a hand. Using flexible velcro strips, the whole mold is suspended from an aluminum strut that extends into the magnetic shield. (C) Four commercial OPM sensors (QuSpin) arranged on a plastic board that is fit to the magnetic shield. (D) Experimental setup showing a participant in a clinical examination room with the 256-channel, high-density EEG cap, the TMS coil in position to stimulate the left primary motor cortex (M1), and forearm inside the magnetic shield. In contrast to a magnetically shielded room-typically required for sensitive biomagnetic measurements, our setup avoids potentially claustrophobic conditions. (E) View inside the innermost shielding layer, with the eight OPMs seen.

larger background fields close or beyond the compensation range of the built-in coils. Therefore OPM eight did not operate at all. The operation of the other sensors was not consistent across subjects and sensors operating close to their compensation limit can produce signals wildly moving around as can be seen in Figure 3C), the faint colored traces. Since fields inside a half open shield can be very inhomogeneous even in a pair of neighboring sensors one might be operable and the second one might experience fields beyond the compensation range.

Data analysis

All of the magnetometer data from each participant were analyzed using a custom Python code for cutting and averaging based on the TMS trigger signal. Notch filters were applied at 50 Hz (Q=20) and higher harmonics, and the data were smoothed with an evenly weighted four-point moving window. The EMG electrode data were extracted and partially analyzed using MNE, an open-source Python software [38, 39].

To establish the robustness of the latency values across trials, a set number of trials were selected at random to be averaged, and a double Gaussian fit with linear offset was made around 25 ms after the trigger on a single channel. The double Gaussian function that the data was fitted to is defined as,

$$y = A_1 \times e^{\frac{-(x-x_1)^2}{2\sigma_1^2}} + A_2 \times e^{\frac{-(x-x_2)^2}{2\sigma_2^2}} + y_0 + m \times x, \quad (1)$$

where A_1 and A_2 are the individual Gaussian amplitudes, x_1 and x_1 and respective offsets, σ_1 and σ_2 are the Gaussian widths, y_0 is an offset and m is the linear slope. The fit parameters y_0 and m capture the decaying artifact from the TMS pulse that overlaps the MEP signal. This fit was chosen as best able to capture the bi-phasic signal and extract a

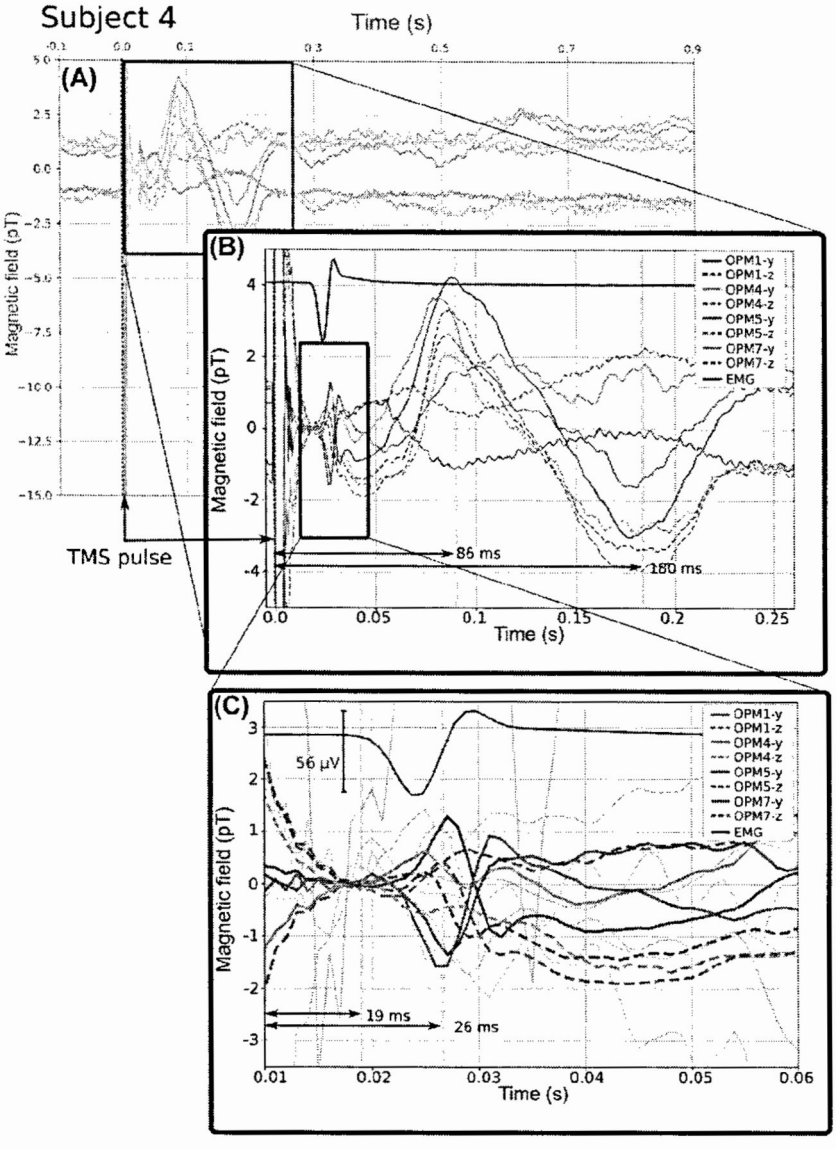

Figure 3: Combined EMG and MMG data for a single participant, showing relative detail in magnetic vs. electric myography, and how the data from three input methods in the experimental system complement each other.
(A) 120 averages of MMG and EMG data before, during and after the TMS pulse (occurring at 0.0 s). Following the large artifact at the TMS pulse, magnetic activity in the hand is detected for approximately 300 ms in this subject, which, based on control measurements, was not attributable to vibration. (B), (C) Zoom of the data in (A) for the time period immediately following the TMS pulse. The magnetic sensors detect both activities which coincides with the electric channel, and which occurs while the electric channel shows nothing. Four of 16 magnetic sensor channels were selected based on noise levels and signal amplitude. Referencing Figure 1A: MMG1, magnetometer OPM7; MMG2, magnetometer OPM4.

consistent value for the latency between the stimulus to the onset of the action potential, but has no particular physical meaning. The 25 ms offset time window was chosen to coincide with the MEP latency and to avoid fitting the artifact.

The latency is then defined as $x_1 - 2.5\sigma_1$ where x_1 is the center offset value of the first fitted Gaussian, and σ_1 is the half-width-half-max of the fit. The value of $2.5\sigma_1$ represents a reliable point at which the data rises above the noise level, defining a consistent value of the latency unbiased by hand-based measurements. This fit was used for both the electric and magnetic data.

Results and discussion

Averaged data resulting from 120 repetitive TMS pulses at 0.5 Hz in a single participant are shown in Figure 3. While 16 magnetic sensor channels are available from the experiment, we select the four shown for clarity and consistency across subjects because some sensors failed (out of range due to environment) during measurements. The sensors shown [y- and z-axes from magnetometers MMG1(OPM7) and MMG2(OPM4)] are positioned below and above the hand, respectively. The signals arising from other sensors are qualitatively similar. In Figure 3A, the signals from both the EMG and MMG are shown to occur within 300 ms of the TMS pulse, with little discernible activity thereafter. During the TMS magnetic artifact, the y and z sensors record large features with the same sign, indicating that fields at these sensors are aligned similarly.

Figure 3B shows a narrower time window. Here, both magnetic and electric (shown in red) channels exhibit a feature at 26 ms, which can be understood as the time for a nerve signal to travel from the motor cortex to the hand. On

the EMG channel, this feature is identified as the MEP [13]. On the MMG channel, the relative sign and shapes of the magnetic features in the data could be used to inform source location of the muscle activity. Starting at around 50 ms after the TMS pulse, the magnetic channels record a bi-phasic feature that lasts up to 200 ms. This larger magnetic signal does not appear on the EMG and the amplitude is not consistent with possible vibration induced signals measured in control trials. Furthermore, it is not visible in artifact measurements either. The loss of this H-reflex signal in EMG recording could be due to the choice of filter parameters implemented in this study [40].

Figure 4 shows the TMS invoked magnetic and electric response of the hand for four subjects. Each subject has a unique magnetic signal – for example, data from Subject 1 shows magnetic field values that are almost three times as large as those of the other subjects. Inter-subject variability during TMS could account for variability in the EMG and MMG recordings [41]. For both EMG and MMG, variability was calculated by removing any constant or linear offsets from the signal and summing the absolute values between the TMS trigger and 500 ms post trigger, calculating the effective area below the signal curves. The variation from the mean (VFM) value of the area is calculated and the

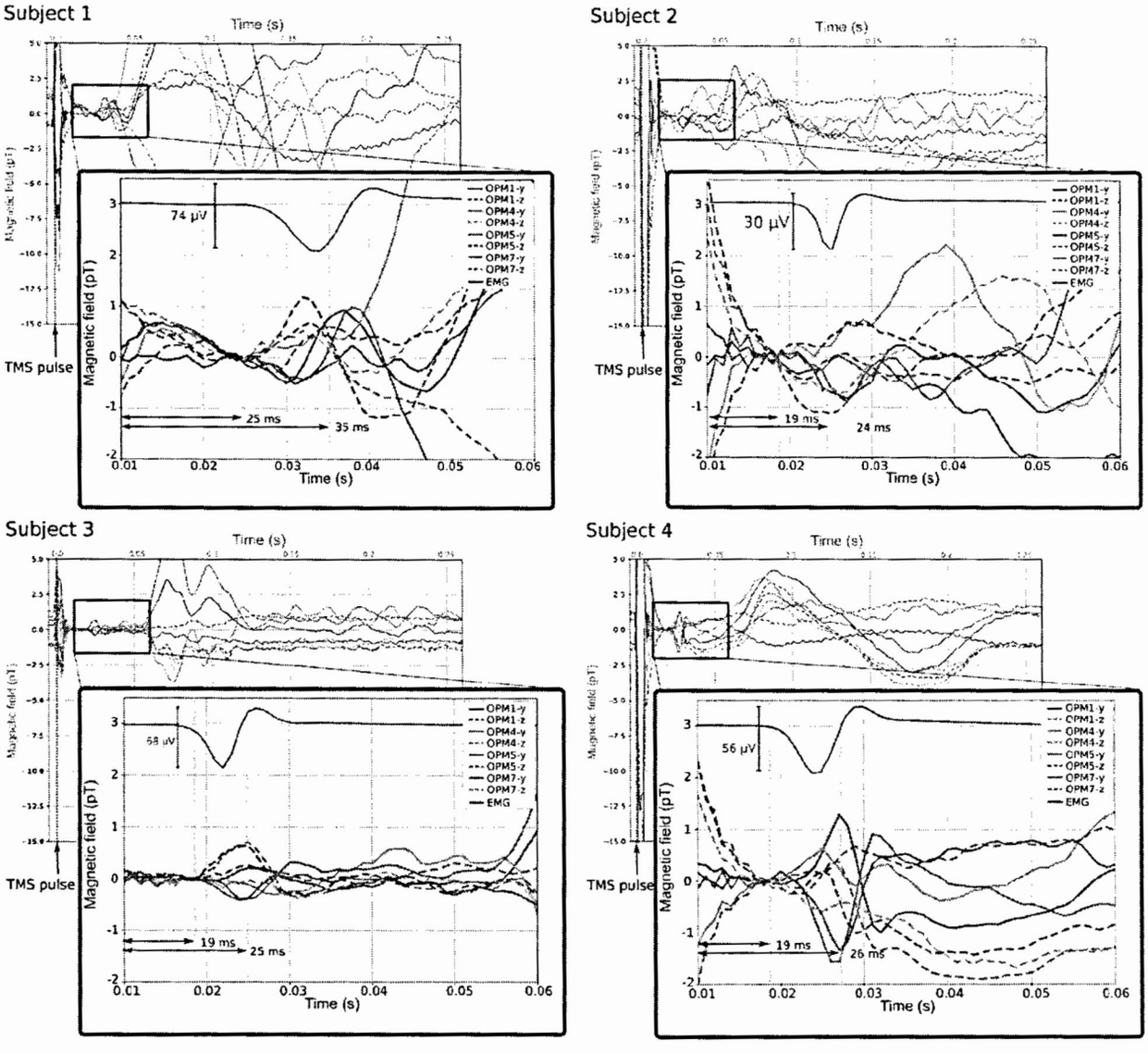

Figure 4: Combined MMG and EMG data for four participants. Variability across subjects is clearly discernible in the MMG data, but all show qualitatively similar results for all signal types. The shape of the TMS artifact is strongly dependent on the position of the coil relative to the magnetic shield, which varies from participant to participant. Additionally, the actual duration of the TMS pulse is ≈300 µs, while the OPM data acquisition rate is 1 kHz without filter. The TMS artifact is distorted due to low sampling, low pass filtering, and a timing jitter between the pulse and the sampling trigger. Note: The EMG electrode from Subject 1 was found afterward to have been improperly grounded, leading to large noise artifacts that remained after filtering and smoothing. Nevertheless, the MEP is still visible.

average variability for all four subjects is 28% for EMG recordings, and 34% for MMG recordings. Variability in the magnetic recordings is greater than that of the EMG, which could result from the fact that the magnetic signal is strongly dependent on the distance between source and sensor, which varied based on the subject morphology. Inter-trial variation could not be calculated because of inadequate signal-to-noise ratio. The poor SNR arises due to operating the OPMs in the open shield, which results in a residual noise amplitude of ≈10 pT.

Data from all the participants show that the MEP from the EMG is detected in the magnetometer channels. Finally, in the EEG we observe qualitatively similar behavior of the brain activity across subjects at the time points chosen based on features in the MMG. We speculate with the new results of the equivalent current dipole analyses the first peak in the EEG topogram is an efferent and the next two peaks are Afferent effects as indicated in Figure 6. The first two MMG peaks shows at shorter intervals are more cortical and either radial (26 ms) and tangential (80 ms), however the dipole for the 180 ms was located in a deeper subcortical region in this case the thalamus. So, we speculate even though the response from thalamus will take not so long to reach the periphery one hint could be that these are more afferent effects. To our knowledge there are no existing literature to record MEP using SQUID. However, in this extensive review [42] the multimodality aspects of EEG-TMS and MEG-TACS to interact with ongoing brain activity are discussed and indicated that simultaneous EEG-TMS is useful for this interrogation. On the other hand, there are several studies reporting similar topography with EEG in relation to the EMG responses as shown in these studies [43, 44].

The robustness in calculating the latency of MEP in the MMG signals is shown in Figure 5. Figure 5A shows that the value for the latency settles to within one standard deviation of the final calculated value (maximum number of averages) within 45 averages. This analysis was used for all subjects.

These data demonstrate the complementarity of MMG to EMG signals in TMS measurements. There is good agreement between the latencies extracted from MMG or EMG measurements (see Table 1), and the magnetic field measurement offers important validations of the electrical potential measurement. For example, EMG data can be influenced by a variety of factors involving the electrode-skin contact, including transient changes such as changing electrode impedance due to increases or decreases in skin moisture during the measurement and changing noise floors [45]. While the specific geometry of the source determines the magnetic field at the sensor, the near unity permittivity of tissue or bone means that it can convey the absolute value of the field from the source and could be used to decouple changing systematic experimental conditions between measurements. In our data set, the MMG data suffers from inadequate SNR to perform such analysis on a trial-by-trial basis, but the signals averaged from 45 trial windows could be compared. MMG can also aid in identifying and locating TMS activated muscles that are not in regions probed by surface electrodes. In this work, the sensor-hand relative positioning was not adequately controlled to perform

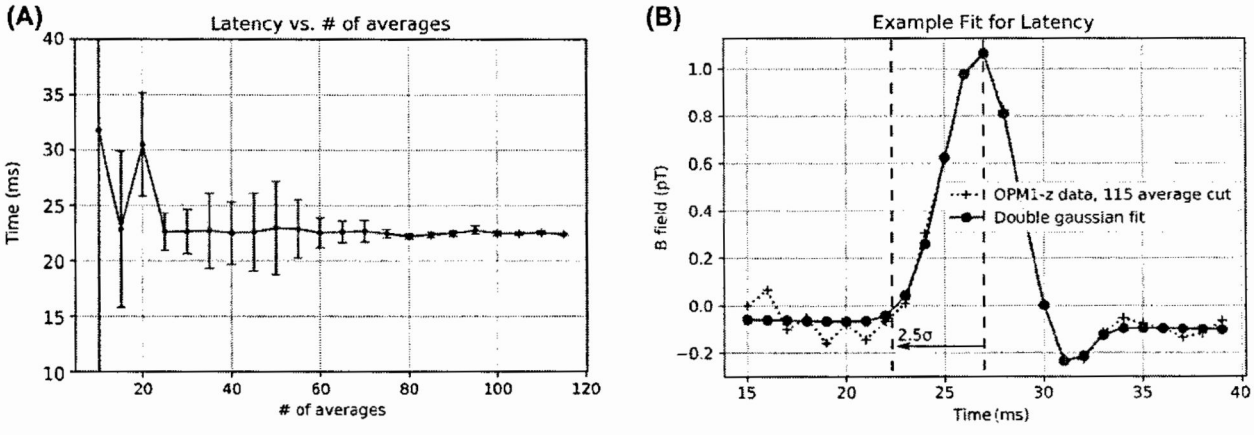

Figure 5: Robustness of latency of magnetic peak recorded near EMG action potential for subject number 4.
(A) Calculated latency vs. number of averages. Latency is calculated by averaging fixed number of random trials and then fitting the magnetic signal data to a bi-phasic peak and extracting the center offset. Latency value falls within 1 standard deviation of final value within 45 averages. (B) Example double Gaussian fit of a 100 trials of magnetic signal from a single channel to find the latency. Latency is defined as 2.5σ prior to the center offset fit of the first Gaussian, where σ is the half-width-half-max.

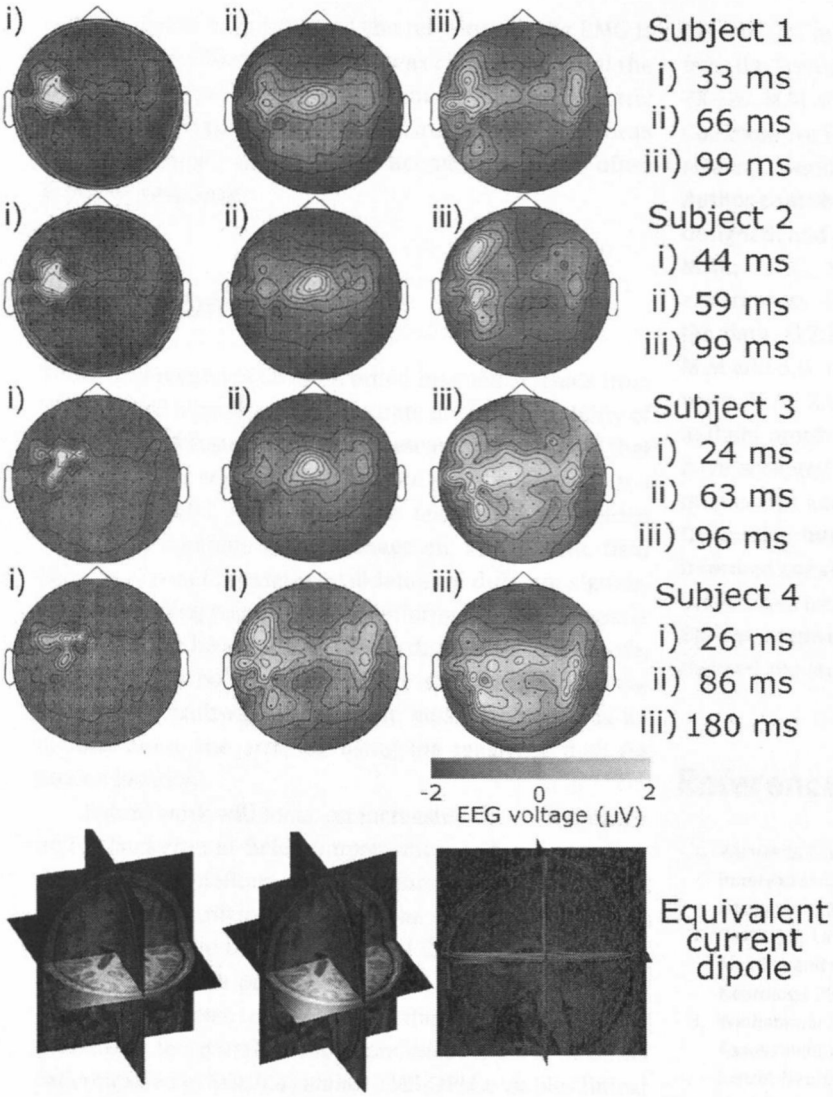

Figure 6: The three peaks found in the MMG signal and their corresponding topograms for each subject separately in each row are shown. The last row shows the equivalent current dipole results for the corresponding three peaks shown in red dipoles. The first peak showed a radial oriented dipole the second and the third dipole showed tangential oriented dipole. The first two peaks showed cortical dipoles in the stimulated motor cortex and the third peak showed a sub-cortical dipole in the thalamus indicating afferent effects.

reliable inversion of the field to acquire the source location. However, future work with better sensor array positioning and hand position indicator methods, similar to head position indicators, could be used to achieve the high resolution widely demonstrated in the literature [46–48]. In addition, a clear drawback in our setup is the relatively large distance between the OPMs and subject's arm/hand. Moreover also the number of trials needed to get a good response with the OPM is a limitation in the current study.

The baseline of the averaged data is calculated in the window from 18 to 19 ms after the stimulus for subjects 2–4 since this is before the peak onset in the EMG. With this baseline a dipolar magnetic response is seen in

Table 1: Comparison of MEP latency from EMG vs. MMG for each subject. Uncertainty, shown in parentheses, was calculated from covariance matrix of the fitted Gaussian function. Uncertainty for the average is standard deviation of the four subjects. For Subject 4, there is a 1σ discrepancy in the timing of the MEP as measured from electric and magnetic channels. The good agreement in the averages indicates that there is no statistically significant systematic over- or under- reporting of one method relative to the other.

	MMG, ms	EMG, ms
Subject 1	26(1)	25(1)
Subject 2	20(2)	20(1)
Subject 3	18(2)	19(2)
Subject 4	22(1)	20(1)
Average	22(3)	21(2)

subjects 3 and 4. In subject 1 the response in the EMG is later and therefore the baseline was chosen later and the magnetic response is consistent with the electric response in Figure 4. A double Gaussian function was used for latency estimation to accommodate the often biphasic response.

Conclusions

These first results of OPM-recorded magnetic signals from TMS-evoked movement demonstrate the future viability of the TMS-OPM system for clinical research. We showed that magnetic field sensing of periphery limbs is possible in a regular hospital room without a magnetically shielded room. The combined use of magnetic and electric field sensors allows for detailed validation of different signals, while providing complementary information about muscle activity in the hand. TMS is targeted, repeatable and safe, and thus can be used in a future study to identify the innervation pathways for specific muscles in various locations along the arm, by using the magnetic data for source location.

Future work will focus on increasing the SNR through active background field compensation and software gradiometry. Well defined sensor positions will enable source localization, further improving the diagnostic aid that MMG can offer to the gold-standard EMG.

Together with portable magnetic shielding, commercial OPM systems can enhance the utility of TMS. In particular, the portable and economical aspects of OPMs (as compared to SQUIDs) makes TMS-OPM a viable clinical tool. This approach represents a new modality in TMS research with opportunities for peripheral nerve study. Additionally, future implementations of this system within head sized shields could enable low cost and accessible magnetoencephalography, furthering research towards better understanding and diagnoses of movement disorders and motor neuron diseases.

Research funding: The work was funded in part by the German Federal Ministry of Education and Research (BMBF) within the Quantumtechnologien program (FKZ 13N14439 and 13N15064) and the Deutsche Forschungsgemeinschaft (DFG) through the DIP program (FO 703/2-1) and the Other Instrumentation-Based Research Infrastructure program (FKZ 324668647). T.S. acknowledges the support of the Core Facility "Metrology of Ultra-Low Magnetic Fields" at Physikalisch-Technische Bundesanstalt, which receives funding from the Deutsche Forschungsgemeinschaft (DFG KO 5321/3-1 and TR 408/11-1). S.G acknowledges support from the Transregional Collaborative Research Center (CRC) TR-128. M.M acknowledges support from the Transregional Collaborative Research Center (CRC) TR-128 and the German research foundation (DFG) MU-4534-1/1.

Author contributions: G.Z.I., Y.H., and A.W. conceived of, designed, and constructed the apparatus. Y.H., G.Z.I., T.S., M.M., V.C.C., S.G, and A.W. prepared and performed the experiments. G.Z.I., Y.H., M.M., Q.L., and V.C.C. analyzed the data. G.Z.I., M.M., and V.C.C. wrote the manuscript. M.M and S.G. advised and informed clinical aspects of the work. M.M, S.G., D.B., and A.W. supervised the work. All authors proofread and edited the manuscript. All authors have accepted responsibility for the entire content of this manuscript and approved its submission.

Competing interests: Authors state no conflict of interest.

Informed consent: Informed consent was obtained from all individuals included in this study.

Ethical approval: The local Institutional Review Board deemed the study exempt from review.

References

1. Wynter S, Dissabandara L. A comprehensive review of motor innervation of the hand: variations and clinical significance. Surg Radiol Anat 2018;40:259–69.
2. Ravits JM, La Spada AR. ALS motor phenotype heterogeneity, focality, and spread: deconstructing motor neuron degeneration. Neurology 2009;73:805–11.
3. Winhammar JM, Rowe DB, Henderson RD, Kiernan MC. Assessment of disease progression in motor neuron disease. Lancet Neurol 2005;4:229–38.
4. Vucic S, Ziemann U, Eisen A, Hallett M, Kiernan MC. Transcranial magnetic stimulation and amyotrophic lateral sclerosis: pathophysiological insights. J Neurol Neurosurg Psychiatry 2013; 84:1161–70.
5. Chou YH, Hickey PT, Sundman M, Song AW, Chen NK. Effects of repetitive transcranial magnetic stimulation on motor symptoms in Parkinson's disease: a systematic review and meta-analysis. JAMA Neurol 2015;72:432–40.
6. Cantello R, Tarletti R, Civardi C. Transcranial magnetic stimulation and Parkinson's disease. Brain Res Rev 2002;38: 309–27.
7. Rossini P, Berardelli A, Deuschl G, Hallett M, Maertens de Noordhout A, Paulus W, et al. Applications of magnetic cortical stimulation. Electroencephalogr Clin Neurophysiol Suppl 1999;52:171–85.
8. Hiraoka K, Horino K, Yagura A, Matsugi A. Cerebellar TMS evokes a long latency motor response in the hand during a visually guided manual tracking task. Cerebellum 2010;9:454–60.
9. Kobayashi M, Pascual-Leone A. Transcranial magnetic stimulation in neurology. Lancet Neurol 2003;2:145–56.
10. Hallett M. Transcranial magnetic stimulation and the human brain. Nature 2000;406:147.

11. Goetz SM, Deng ZD. The development and modelling of devices and paradigms for transcranial magnetic stimulation. Int Rev Psychiatr 2017;29:115–45.
12. Rossini PM, Rossi S. Transcranial magnetic stimulation: diagnostic, therapeutic, and research potential. Neurology 2007; 68:484–8.
13. Groppa S, Oliviero A, Eisen A, Quartarone A, Cohen LG, Mall V, et al. A practical guide to diagnostic transcranial magnetic stimulation: report of an IFCN committee. Clin Neurophysiol 2012; 123:858–82.
14. McMackin R, Muthuraman M, Groppa S, Babiloni C, Taylor JP, Kiernan MC, et al. Measuring network disruption in neurodegenerative diseases: new approaches using signal analysis. J Neurol Neurosurg Psychiatr 2019;90:1011–20.
15. Tassinary LG, Cacioppo JT, Vanman EJ. The skeletomotor system: surface electromyography. In: Cacioppo JT, Tassinary LG, Berntson GG, editors. Handbook of psychophysiology. New York, NY: Cambridge University Press; 2007:267–99 pp.
16. Cohen D, Givler E. Magnetomyography: magnetic fields around the human body produced by skeletal muscles. Appl Phys Lett 1972;21:114–6.
17. Masuda T, Endo H, Takeda T. Magnetic fields produced by single motor units in human skeletal muscles. Clin Neurophysiol 1999; 110:384–9.
18. Reaz MBI, Hussain MS, Mohd-Yasin F. Techniques of EMG signal analysis: detection, processing, classification and applications. Biol Proced Online 2006;8:11–35.
19. Mosher JC, Lewis PS, Leahy RM. Multiple dipole modeling and localization from spatio-temporal MEG data. IEEE Trans Biomed Eng 1992;39:541–57.
20. Schenck JF. The role of magnetic susceptibility in magnetic resonance imaging: MRI magnetic compatibility of the first and second kinds. Med Phys 1996;23:815–50.
21. Williamson SJ, Romani GL, Kaufman L, Modena I. Biomagnetism: an interdisciplinary approach. Berlin, Germany: Springer Science & Business Media; 2013, 66.
22. Weinstock H. SQUID sensors: fundamentals, fabrication and applications. Berlin, Germany: Springer Science & Business Media; 2012, 329.
23. Grimes D, Lennard R, Swithenby S. DC magnetic fields of the human leg as a function of position and relaxation. Il Nuovo Cimento D 1983;2:650–9.
24. Drung D. The PTB 83-SQUID system for biomagnetic applications in a clinic. IEEE Trans Appl Supercond 1995;5:2112–7.
25. Burghoff M, Albrecht HH, Hartwig S, Hilschenz I, Körber R, Sander-Thömmes T, et al. SQUID system for MEG and low field magnetic resonance. Metrol Meas Syst 2009;16:371–6.
26. Allred J, Lyman R, Kornack T, Romalis M. High-sensitivity atomic magnetometer unaffected by spin-exchange relaxation. Phys Rev Lett 2002;89:130801.
27. Shah VK, Wakai RT. A compact, high performance atomic magnetometer for biomedical applications. Phys Med Biol 2013; 58:8153.
28. Masuyama Y, Suzuki K, Hekizono A, Iwanami M, Hatano M, Iwasaki T, et al. Gradiometer using separated diamond quantum magnetometers. Sensors 2021;21:977.
29. Boto E, Holmes N, Leggett J, Roberts G, Shah V, Meyer SS, et al. Moving magnetoencephalography towards real-world applications with a wearable system. Nature 2018;555:657.
30. Broser PJ, Knappe S, Kajal DS, Noury N, Alem O, Shah V, et al. Optically pumped magnetometers for magneto-myography to study the innervation of the hand. IEEE Trans Neural Syst Rehabil Eng 2018;26:2226–30.
31. Elzenheimer E, Laufs H, Schulte-Mattler W, Schmidt G. Magnetic measurement of electrically evoked muscle responses with optically pumped magnetometers. IEEE Trans Neural Syst Rehabil Eng 2020;28:756–65.
32. Broser PJ, Middelmann T, Sometti D, Braun C. Optically pumped magnetometers disclose magnetic field components of the muscular action potential. J Electromyogr Kinesiol 2021;56: 102490.
33. Richter L, Neumann G, Oung S, Schweikard A, Trillenberg P. Optimal coil orientation for transcranial magnetic stimulation. PLoS One 2013;8:e60358.
34. Cavaleri R, Schabrun SM, Chipchase LS. The number of stimuli required to reliably assess corticomotor excitability and primary motor cortical representations using transcranial magnetic stimulation (TMS): a systematic review and meta-analysis. Syst Rev 2017;6:48–8.
35. Barker AT, Jalinous R, Freeston IL. Non-invasive magnetic stimulation of human motor cortex. Lancet 1985;325:1106–7.
36. Boto E, Meyer SS, Shah V, Alem O, Knappe S, Kruger P, et al. A new generation of magnetoencephalography: room temperature measurements using optically-pumped magnetometers. Neuroimage 2017;149:404–14.
37. Sullivan GW, Lewis P, George J, Flynn E. A magnetic shielded room designed for magnetoencephalography. Rev Sci Instrum 1989; 60:765–70.
38. Gramfort A, Luessi M, Larson E, Engemann DA, Strohmeier D, Brodbeck C, et al. MEG and EEG data analysis with MNE-Python. Front Neurosci 2013;7:267.
39. Gramfort A, Luessi M, Larson E, Engemann DA, Strohmeier D, Brodbeck C, et al. MNE software for processing MEG and EEG data. Neuroimage 2014;86:446–60.
40. Christie A, Kamen G, Boucher JP, Greig Inglis J, Gabriel DA. A comparison of statistical models for calculating reliability of the Hoffmann Reflex. Meas Phys Educ Exerc Sci 2010;14:164–75.
41. Kiers L, Cros D, Chiappa K, Fang J. Variability of motor potentials evoked by transcranial magnetic stimulation. Electroencephalogr Clin Neurophysiology Evoked Potentials Sect 1993;89:415–23.
42. Thut G, Bergmann TO, Fröhlich F, Soekadar SR, Brittain JS, Valero-Cabré A, et al. Guiding transcranial brain stimulation by EEG/MEG to interact with ongoing brain activity and associated functions: a position paper. Clin Neurophysiol 2017;128:843–57.
43. Bergmann TO, Mölle M, Schmidt MA, Lindner C, Marshall L, Born J, et al. EEG-guided transcranial magnetic stimulation reveals rapid shifts in motor cortical excitability during the human sleep slow oscillation. J Neurosci 2012;32:243–53.
44. Schilberg L, Ten Oever S, Schuhmann T, Sack AT. Phase and power modulations on the amplitude of TMS-induced motor evoked potentials. PLoS One 2021;16:e0255815.

45. Huigen E, Peper A, Grimbergen CA. Investigation into the origin of the noise of surface electrodes. Med Biol Eng Comput 2002;40: 332–8.
46. Borna A, Carter TR, Colombo AP, Jau YY, McKay J, Weisend M, et al. Non-invasive functional-brain-imaging with an OPM-based magnetoencephalography system. PLoS One 2020;15:e0227684.
47. Zetter R, Iivanainen J, Parkkonen L. Optical co-registration of MRI and on-scalp MEG. Sci Rep 2019;9:1–9.
48. Hämäläinen M, Hari R, Ilmoniemi RJ, Knuutila J, Lounasmaa OV. Magnetoencephalography—theory, instrumentation, and applications to noninvasive studies of the working human brain. Rev Mod Phys 1993;65:413.